

# A Decade in the Life of EXO 2030+375: A Multi-wavelength Study of an Accreting X-ray Pulsar

Colleen A. Wilson<sup>1</sup>, Mark H. Finger<sup>2</sup>

*SD 50 Space Science Research Center, National Space Science and Technology Center, 320 Sparkman Drive, Huntsville, AL 35805*

colleen.wilson-hodge@msfc.nasa.gov

M.J. Coe, Silas Laycock

*Dept. of Physics and Astronomy, The University, Southampton, SO17 1BJ, England*

J. Fabregat

*Dept d'Astronomia i Astrofísica, Universitat de València, 46100 Burjassot, València, Spain*

## ABSTRACT

Using BATSE and *RXTE* observations from 1991 April to 2001 August we have detected 71 outbursts from 82 periastron passages of EXO 2030+375, a 42-second transient X-ray pulsar with a Be star companion, including several outbursts from 1993 August to 1996 April when the source was previously believed to be quiescent. Combining BATSE, *RXTE*, and *EXOSAT* data we have derived an improved orbital solution. Applying this solution results in a smooth profile for the spin-up rate during the giant outburst and results in evidence for a correlation between the spin-up rate and observed flux in the brighter BATSE outbursts. Infrared and  $H\alpha$  measurements show a decline in the density of the circumstellar disk around the Be star. This decline is followed by a sudden drop in the X-ray flux and a turn-over from a spin-up trend to spin-down in the frequency history. This is the first Be/X-ray binary which shows an extended interval, about 2.5 years, where the global trend is spin-down, but the outbursts continue. In 1995 the orbital phase of EXO 2030+375's outbursts shifted from peaking about 6 days after periastron to peaking before periastron. The outburst phase slowly recovered to peaking at about 2.5 days after periastron. We interpret this shift in orbital phase followed by a slow recovery as evidence for a global one-armed oscillation propagating in the Be disk. This is further supported by changes in the shape of the  $H\alpha$  profile which are commonly believed to be produced by a reconfiguration of the Be disk. The truncated viscous decretion disk model provides an explanation for the long series of normal outbursts and the evidence for an accretion disk in the brighter normal outbursts. Long-term multi-wavelength observations such as these clearly add considerably to our knowledge of Be/X-ray binaries and the relationship between optical, infrared and X-ray observations.

*Subject headings:* accretion—stars:pulsars:individual:(EXO 2030+375)—X-rays: binaries

---

<sup>1</sup>NASA's Marshall Space Flight Center

<sup>2</sup>Universities Space Research Association

## 1. Introduction

Be/X-ray binaries are the most common type of accreting X-ray pulsar systems. They consist of a

pulsar and a Be (or Oe) star, a main sequence star of spectral type B (or O) that shows Balmer emission lines (See e.g., Slettebak 1988 and Apparao 1994 for reviews.) The line emission is believed to be associated with an equatorial outflow of material expelled from the rapidly rotating Be star that probably forms a quasi-Keplerian disk near the Be star (Quirrenbach et al. 1997; Hanuschik 1996). X-ray outbursts are produced when the pulsar interacts with this disk. Be/X-ray binaries typically show two types of outburst behavior: (a) giant outbursts (or type II), characterized by high luminosities ( $L_X \gtrsim 10^{37}$  ergs  $s^{-1}$ ) and high spin-up rates (i.e., a significant increase in pulse frequency) and (b) normal outbursts (or type I), characterized by lower luminosities ( $L_X \sim 10^{36} - 10^{37}$  ergs  $s^{-1}$ ), low spin-up rates (if any), and recurrence at the orbital period (Stella, White, & Rosner 1986; Bildsten et al. 1997). As a population Be/X-ray binaries show a correlation between their spin and orbital periods (Corbet 1986; Waters & van Kerkwijk 1989).

EXO 2030+375 is a 42-second transient accreting X-ray pulsar discovered during a giant outburst in 1985 with *EXOSAT* (Parmar et al. 1989). Optical and infrared observations of the *EXOSAT* error circle identified a B0 Ve star as the most likely companion (Motch & Janot-Pacheco 1987; Janot-Pacheco, Motch, & Pakull 1988; Coe et al. 1988). The initial outburst was first detected at a 1-20 keV luminosity of  $1 \times 10^{38}$  ergs  $s^{-1}$  (using a distance of 5 kpc assumed by Parmar et al. 1989) on 1985 May 18 and declined to  $\lesssim 3.8 \times 10^{34}$  ergs  $s^{-1}$  by 1985 August 25. During this luminosity decline, the intrinsic spin period changed dramatically, with a characteristic spin-up timescale  $-P/\dot{P} \approx 30$  yr (Parmar et al. 1989). This large intrinsic spin-up suggested that an accretion disk was present and made determination of an orbit difficult, resulting in 3 acceptable orbits. The rate of change of pulse period  $\dot{P}$  (Parmar et al. 1989), the energy spectrum (Reynolds, Parmar, & White 1993; Sun et al. 1994) and the 1-10 keV pulse profile (Parmar, White, & Stella 1989) all showed significant luminosity dependence. Further evidence of an accretion disk resulted from the detection of 0.2 Hz quasi-periodic oscillations (Angelini, Stella, & Parmar 1989) consistent with the magnetospheric beat frequency model (Lamb et al. 1985) and the Keplerian frequency model (van der Klis

et al. 1987). A second outburst, roughly a factor of 10 weaker in luminosity than the first, was also detected with *EXOSAT* in 1985 October 28-November 3 (Parmar et al. 1989). This outburst was apparently a normal outburst, but it showed unusual flaring activity. These flares were detected on 1985 October 30-31 and had a 4 hour recurrence period (Parmar et al. 1989; Apparao 1991). Observations of EXO 2030+375 were quite sparse for the next several years. *Ginga* observed EXO 2030+375 on 1989 October 29-31 and 1991 October 24 (Sun et al. 1992). Pulsations were detected only in the 1989 observations, with an observed pulse period of 41.68202(8) s and an observed period derivative of  $\dot{P} = -(8.3 \pm 0.9) \times 10^{-9}$  s/s at MJD 47828.95. EXO 2030+375 was also detected in the soft X-ray band for two days near a periastron passage with *ROSAT* in November 1990 (Mavromatakis 1994); however the observations, short 10-28 s scans, were not suitable to detect pulsations.

The most extensive observations of EXO 2030+375 were made with the Large Area Detectors (LADs) of the Burst and Transient Source Experiment (Fishman et al. 1989, BATSE) on the *Compton Gamma Ray Observatory (CGRO)*. From launch in April 1991 until *CGRO* was de-orbited in June 2000, BATSE provided nearly continuous coverage of EXO 2030+375. During the interval 1992 February 8-1993 August 26, 13 consecutive outbursts of EXO 2030+375 were seen with peak luminosities of  $0.3 \times 10^{37} \leq L_{X \ 1-20 \text{ keV}} \leq 3.0 \times 10^{37}$  ergs  $s^{-1}$  (See Stollberg et al. 1999 for spectral assumptions), durations of 7-19 days, and spacings of 46 days (Bildsten et al. 1997; Stollberg et al. 1999). These outbursts peaked 5-6 days after periastron passage. A few detections of marginal statistical significance preceded and followed this sequence of outbursts. During the 13 outbursts, the pulsar spun-up at an average rate of  $1.3 \times 10^{-13}$  Hz  $s^{-1}$ . The 20-160 keV pulse profiles were double peaked and showed no significant energy or luminosity dependence. A binary orbit listed in the top row of Table 2 was determined using these 13 outbursts (Stollberg et al. 1999). Near simultaneous optical, infrared, and X-ray observations of an outburst in 1993 June/July showed no significant evidence for a correlation between X-ray flux and infrared luminosity or between the X-ray flux and the equivalent width, strength, or profile of the H $\alpha$

emission line (Norton et al. 1994). EXO 2030+375 was not detected above a flux level of  $\sim 4.2 \times 10^{-10}$  ergs  $\text{cm}^{-2} \text{s}^{-1}$  (20-50 keV) in the search techniques used from 1993 August 26 to 1996 April. Beginning in 1996 April, three short, weak, outbursts were detected with BATSE, separated by 46 days (Stollberg et al. 1996, 1999). These outbursts began about 5 days prior to periastron passage as predicted using the orbital model of Stollberg et al. (1999). Outbursts were also regularly detected with the All-Sky Monitor (Levine et al. 1996, ASM) on the *Rossi X-ray Timing Explorer* (*RXTE*) beginning in 1996 March (Reig & Coe 1998).

An outburst of EXO 2030+375 was observed from 1996 July 1-10 with the *RXTE* Proportional Counter Array (Jahoda et al. 1996, PCA). Pulsations were detected throughout the observations. This outburst began about 5 days prior to periastron passage. The 2-10 keV pulse profile did not show significant intensity dependence. In fact, it was consistent with the 1-10 keV *EXOSAT* profile observed at a similar luminosity (Reig & Coe 1998). The energy spectrum was correlated with luminosity (Reig & Coe 1999). This correlation was consistent with an extrapolation of that observed in *EXOSAT* data by Reynolds, Parmar, & White (1993). Evidence for a possible cyclotron feature at 36 keV was found in spectra from the High Energy X-ray Timing Experiment (Rothschild et al. 1998, HEXTE) on *RXTE* (Reig & Coe 1999).

In this paper we will present an improved orbit determination for EXO 2030+375 using BATSE, *RXTE*, and *EXOSAT* data. This improved orbit along with more sensitive search techniques has led to the detection of pulsations in 52 outbursts in 9 years of BATSE data, including several outbursts in the period 1993 August to 1996 April when the source was previously believed to be quiescent. Evidence for 19 additional outbursts, including 10 missed with BATSE and 9 after *CGRO* was de-orbited, was observed with the *RXTE* ASM, for a total of 71 outbursts observed out of 82 periastron passages from 1991 April to 2001 August. We show that our improved orbital parameters remove the two intervals of enhanced spin-up observed by Reynolds et al. (1996) in the initial *EXOSAT* outburst, when they used the orbit of Stollberg et al. (1994) to correct the observed pulse periods. We

also show evidence for a correlation between spin-up rate and flux in the BATSE data and compare it to that observed in the *EXOSAT* data. We compare our X-ray results to optical and infrared observations and discuss evidence for a decline in the density of the Be disk and its effects on the X-ray flux and pulsed frequency histories. We discuss evidence in both optical observations of  $\text{H}\alpha$  profiles and X-ray observations that suggests a global one-armed oscillation (i.e., a density perturbation) was propagating in the Be disk. Lastly, we discuss our observations of EXO 2030+375 in context of current models.

## 2. Analyses and Results

### 2.1. Discovery of Weak Outbursts with BATSE

In previous studies with BATSE (Bildsten et al. 1997; Stollberg et al. 1999), histories of pulse frequency and pulsed flux for known pulsars were generated using grid searches over a range of candidate frequencies. The best fit frequency was determined using the  $Z_n^2$  statistic (Buccheri et al. 1983). These studies were often limited to 1-day integrations by systematic effects. We have developed an “advanced” pulsar search that reduces 3 systematic effects: (1) aperiodic noise from sources in the BATSE field of view, (2) Earth occultations of bright sources during the folding interval, and (3) bright pulses from other pulsars in the BATSE field of view. This technique is described in detail in Finger et al. (1999) and Wilson-Hodge (1999). We will summarize it here, highlighting the differences from previous techniques.

The “advanced” pulsar search technique consists of 3 steps (1) data selection and combination, (2) 20-50 keV pulse profile estimates, and (3) a grid search in frequency. First the BATSE DISCLA channel 1 (20-50 keV, 1 s time resolution data) were selected for which the source was visible, the high voltage was on, the spacecraft was outside the South Atlantic Anomaly, and no electron precipitation events or other anomalies were flagged by the BATSE mission operations team. The count rates were combined over the 4 LADs viewing EXO 2030+375 using weights optimized for an exponential energy spectrum,  $f(E) = A \exp(-E/kT)$  with temperature  $kT = 20$  keV (Stollberg et al. 1999), and grouped

into  $\approx 300$  s segments. A segment length of 300 s was used because it included several pulse periods, but was short enough that the background was well-fitted by a quadratic model. The segment boundaries were chosen to avoid Earth occultation steps from bright sources because these steps could produce spurious signals at high harmonics of the spacecraft orbital period which could overwhelm the real signal, especially for long period pulsars. In the technique previously used by Bildsten et al. (1997) and Stollberg et al. (1999) potentially bright sources were input manually, which worked well for persistently bright sources, e.g., Crab or Cygnus X-1, but not as well for transient sources. Effects from bright transients were greatly reduced in our advanced monitor by maintaining a database that included which sources were active on a given day and what level they were active. Depending upon the pulse period of the source, i.e., which spacecraft harmonic it was closest to, we automatically determined which occultation steps should be avoided in the selection of segment boundaries.

The second step in this process was estimation of an initial 20-50 keV pulse profile for each segment. In each segment, the combined rates were fitted with a model consisting of a sixth-order Fourier expansion in pulse phase model (representing the 20-50 keV pulse profile) and a spline function with quadratics in time (representing the background plus mean source count rate). A sixth-order Fourier expansion was chosen based on the number of harmonics that are significant in a 1-day observation. Our initial pulse phase model was of the form  $\phi(t^{\text{em}}) = \nu_0(t^{\text{em}} - t_0)$ , where  $\nu_0 = 23.9954$  mHz was a constant barycentric frequency and  $t^{\text{em}}$  was the emission time corrected to the pulsar reference frame using the JPL DE-200 ephemeris (Standish et al. 1992) and the orbital parameters from Stollberg et al. (1999). The value and slope of the spline function were required to be continuous across adjacent segment boundaries, but not across data gaps.

The final step in our advanced pulsar search was a grid search in frequency using the set of typically several hundred estimated 20-50 keV pulse profiles from 4-day intervals of data. New EXO 2030+375 pulse frequencies were determined from an initial grid search over 201 evenly spaced trial barycentric frequencies in the range 23.97925-24.00240

mHz. Aperiodic noise from Cygnus X-1 caused the variances on the Fourier coefficients to be larger than expected for Poisson statistics. In previous searches (Bildsten et al. 1997), this caused the  $Z_n^2$  statistic and BATSE's sensitivity to be dependent on the noise level since only the Poisson level was assumed. Stollberg et al. (1999) attempted to account for aperiodic noise from Cygnus X-1 using the average Cygnus X-1 noise level from a single day; however, the noise level from Cygnus X-1 is highly variable (Crary et al. 1996). Hence to better account for the aperiodic noise, its effect must be estimated for each frequency measurement. To correct the Poisson variances on the Fourier amplitudes at each harmonic<sup>3</sup> for aperiodic noise in the power spectrum, we first computed the mean harmonic amplitudes, i.e., mean 20-50 keV pulse profile, for each 4-day interval. Then we computed the reduced  $\chi^2$  of a fit for each harmonic in the mean 20-50 keV pulse profile, to those from the 300-s segments within each 4-day interval. The variances for each harmonic of the mean 20-50 keV pulse profile were then multiplied by this reduced  $\chi^2$ . Due to the large field-of-view of BATSE, other pulsars are often also present when we are measuring EXO 2030+375. If we limit our statistic to use the first 3 harmonics where EXO 2030+375 is the brightest, we reduce the chances of contamination of the search results from other pulsars that happen to have harmonics near the higher harmonics of EXO 2030+375. However, once we know the pulse frequency well and are no longer searching, these harmonics can be re-included to improve the resolution of features in the 20-50 keV pulse profile. A modified  $Z_3^2$  statistic, which we will call  $Y_3$  after Finger et al. (1999), was then computed which incorporated the corrected variances. The reduced  $\chi^2$  used to correct the variances on the first 2 Fourier amplitudes was  $> 2$  for the extended intervals MJD<sup>4</sup> 48361-48650 (1991 Apr - 1992 Jan), 49700-50000 (1994 Dec - 1995 Oct), 50400-50600 (1996 Nov - 1997 Jun), 50650-50950 (1997 Jul - 1998 May), and several shorter intervals indicating increased noise from Cygnus X-1. The best-fit frequency for each 4-day interval was determined using the  $Y_3$  statistic. The root-mean-squared (rms) pulsed flux was then estimated from

<sup>3</sup>In this paper, harmonics are defined as  $n\nu$  where  $n = 1, 2, 3, \dots$  and  $\nu$  is the pulse frequency.

<sup>4</sup>MJD = Julian Date - 2400000.5

the best-fit 20-50 keV pulse profile as (Bildsten et al. 1997, Equation B9)

$$F_{\text{RMS}} = \left[ 0.5 \sum_{k=1}^m (A_k^2 + B_k^2) \right]^{1/2} \quad (1)$$

where  $A_k$  and  $B_k$  are the real and imaginary Fourier coefficients for each harmonic.

Figure 1, panels (a) and (b), illustrate the sensitivity improvements in our new techniques. Panel (a) shows the barycentered, orbit corrected pulse frequencies measured at 1-day intervals from Bildsten et al. (1997) plus a few later outbursts detected using a similar method. In that technique, systematic effects dominated statistical errors for EXO 2030+375, resulting in little improvement in sensitivity for 4-day intervals versus 1-day intervals. Panel (b) shows the barycentered, orbit corrected pulse frequencies measured at 4-day intervals from our new search. Accounting for systematic effects now allows us to combine 4-day intervals with near-statistic errors, resulting in considerable improvement in sensitivity. Our new search revealed many more outbursts than had been previously detected, including several during the 2.5 year “quiescent” interval (Bildsten et al. 1997) 1993 August - 1996 April (MJD 49225-50175). However, there was considerable unexpected scatter in the pulse frequency measurements, starting during the so-called “quiescent” interval. These outbursts were occurring at an earlier orbital phase than those used by Stollberg et al. (1999) to determine the orbit.

## 2.2. Orbit Fitting

We suspected that the scatter in the detected pulse frequencies might be produced by errors in the orbital parameters caused by coupling between the intrinsic spin variations of the pulsar with orbital effects. The different orbital phase of the later outbursts gave us more orbital coverage, improving our ability to decouple these effects. One outburst in 1996 July (MJD 50265-50275) was also observed with the *RXTE* PCA (Reig & Coe 1998, 1999). Barycentered Standard 1 (125 ms, no energy resolution) data were fitted with a model consisting of a constant background plus a sixth-order Fourier expansion in pulse phase model, creating an estimated 2-60 keV pulse profile for each PCA observation. The pulsed phase model consisted

of a constant barycentric frequency  $\nu_0 = 23.9942$  estimated from BATSE measurements and the orbital parameters of Stollberg et al. (1999). The rms pulsed fluxes were computed using Equation 1 for each 2-60 keV profile. The 2-60 keV pulse profile with the brightest pulsed flux from MJD 50268.835-50268.867 (1996 July 4) was selected as the template profile. Phase offsets to the constant frequency model were generated by cross-correlating the 2-60 keV pulse profiles from each observation with the template. Initially we suspected an error in the orbital period, which would show up as an error in the projected epoch of periastron. To test this idea, we fitted the *RXTE* pulse phases with a quadratic phase model and an orbit with the period fixed. The first and second rows in Table 2 list the Stollberg et al. (1999) and our orbital parameters, respectively. Surprisingly, the epoch of periastron passage,  $T_{\text{peri}}$ , was consistent (within  $1\sigma$ ) with the value from Stollberg et al. (1999) propagated to the epoch of the *RXTE* observations. However, the eccentricity  $e$ , the projected semi-major axis  $a_x \sin i$ , and the periastron angle  $\omega$  all shifted slightly, by  $2.2\sigma$ ,  $1.0\sigma$ , and  $2.2\sigma$ , respectively. Although these shifts were small, when we reran the frequency search using the revised orbital parameters, the frequency history no longer showed unexpected scatter.

To better refine the orbital parameters, we generated pulse phase measurements at 1-day intervals using BATSE data for all outbursts detected in our initial search. Table 1 lists the dates of the outbursts we detected. Following steps 1 and 2 of the advanced pulsar search (see Section 2.1), we generated estimated 20-50 keV pulse profiles for 300-s segments using a pulse phase model consisting of a constant barycentric frequency for each outburst. For each 1-day interval, we computed a mean 20-50 keV pulse profile with variances corrected for aperiodic noise using techniques described in Section 2.1 and Finger et al. (1999). To better resolve features in the 20-50 keV pulse profiles, we retained all 6 harmonics. Phase offsets to the pulse phase model were generated by cross-correlating individual 20-50 keV pulse profiles with a template profile. The template profile was the best-fit 20-50 keV profile from the brightest 4-day interval (MJD 49126-49130, 1993 May 19-23) in our frequency search. Pulsed fluxes in the 20-50 keV band were computed for each 1-

day interval using Equation 1. Previous studies (Stollberg et al. 1996; Bildsten et al. 1997; Reig et al. 1998) reported that the outburst observed in 1996 April (MJD 50176-50183) occurred at an earlier orbital phase than the 13 outbursts used by Stollberg et al. (1999) to determine an orbit. Comparing Figures 1 and 9 (described in detail in Section 2.4), one sees that the outbursts where the pulse frequencies show additional scatter, MJD 50000-51000 (1995 Oct - 1998 Jul), are occurring at a much earlier orbital phase than the 13 outbursts (MJD 48659-49228, 1992 Feb - 1993 Aug) used by Stollberg et al. (1999) to determine orbital parameters, suggesting that fitting these outbursts would result in improved orbital parameters. Pulse phase measurements from BATSE and *RXTE* PCA were fitted with a global orbit plus a different quadratic for each outburst using the Levenberg-Marquardt method for  $\chi^2$  minimization. The best fit orbital parameters using the *RXTE* PCA data only, the *RXTE* PCA data plus the 13 outbursts used by Stollberg et al. (1999), and all 53 outbursts detected using the *RXTE* PCA and BATSE are listed in Table 2. Although our pulse phase model does not fully describe the intrinsic pulse frequency variations, the different orbital phase coverage of the *RXTE* PCA observations and the later BATSE outbursts allow better decoupling of orbital and intrinsic torque effects.

Figure 1, panel (c), shows the barycentered and orbit corrected (using Table 2 row 5) 4-day pulse frequency measured with BATSE (*filled circles*) and *RXTE* (*diamonds*). Comparing the panels (b) and (c) of Figure 1 indicates that the new orbital parameters removed the scatter in the frequencies from MJD 50000-51000 (1995 Oct - 1998 Jul). Also, in panel (c), there are 4 additional detected frequencies above 99.9% confidence. The bottom panel shows the 20-50 keV pulsed flux history measured with BATSE assuming an exponential energy spectrum with  $kT = 20$  keV. Monte Carlo simulations were run to determine detection confidence levels. From  $10^4$  trials, we determined detection confidence levels of 99% ( $Y_3 \gtrsim 26.8$ ) and 99.9% ( $Y_3 \gtrsim 32.5$ ). In Figure 1 (bottom panel), detections ( $\gtrsim 99.9\%$  confidence) are denoted using filled circles and 99% confidence upper limits on the 20-50 keV pulsed flux for the periastron passages where BATSE did not detect pulsations from EXO 2030+375 are denoted by arrows.

To further improve our orbital model, we decided to revisit the *EXOSAT* observations of the initial giant outburst. We downloaded 1-8 keV background subtracted *EXOSAT* light curves from the Medium Energy (ME) proportional counter (Turner et al. 1981) with 1 second time resolution from the High Energy Astrophysics Science Archive Research Center (HEASARC)<sup>5</sup> at Goddard Space Flight Center for 14 *EXOSAT* observations (Parmar et al. 1989, for observation details). We were unable to unambiguously maintain a pulsar cycle count across these observations, so we measured pulse frequencies instead. For each observation, we fitted a model consisting of a constant plus a 6 harmonic Fourier expansion in a pulse phase model which incorporated the orbit listed in the fourth row of Table 2. The position history of the *EXOSAT* spacecraft versus time was not available, so we corrected to the solar system barycenter assuming a fixed spacecraft position. Effects of the spacecraft motion are expected to be small relative to the measurement errors. We searched over a grid of 101 evenly spaced pulse frequencies in the range 23.881-23.997 mHz. The best-fit frequency was selected using a method similar to that used with BATSE data. In this case, the aperiodic noise level was estimated by first extracting and then averaging the Leahy normalized (Leahy et al. 1983) power spectra for all available 1 ksec intervals of contiguous data in each observation. The variances on the  $n$ -harmonic amplitudes were multiplied by the ratio  $\bar{P}_n/P_{\text{Poisson}}$ , where  $\bar{P}_n$  is the average power in the frequency range  $n\nu/2$  to  $3n\nu/2$  and  $P_{\text{Poisson}} = 2$  is assumed. The  $Y_6$  statistic was then computed for each frequency in the grid for each observation. We confidently detected pulsations in all of the 14 observations except the observation on 1985 August 25, when Parmar et al. (1989) also failed to detect pulsations.

Reynolds et al. (1996) corrected the *EXOSAT* pulse frequency measurements using the orbital parameters of Stollberg et al. (1994). They reported that the spin-up trend in the intrinsic frequencies was not smooth, steepening temporarily between the 1985 May 29 (MJD 46214) and June 4 (MJD 46220) observations, and again between July 10 (MJD 46256) and 25 (MJD 46271).

<sup>5</sup><http://heasarc.gsfc.nasa.gov>

They speculated that this steepening could be due to errors in the orbital parameters. When we used our new orbital parameters from BATSE and *RXTE* data to correct the pulse frequencies, these changes in spin-up trend were reduced, but not completely removed. The *EXOSAT* data covered orbital phases not included in any BATSE or *RXTE* detections of EXO 2030+375. We decided to attempt an additional orbital fit to the combined data set, including *EXOSAT* observed pulse frequencies from the initial giant outburst, BATSE pulse phases for 51 outbursts, and *RXTE* PCA pulse phases for 2 outbursts (1996 July and 3 observations spanning 1998 January 8-15). The fitting model consisted of a global orbit, a third order polynomial intrinsic pulse frequency model for the *EXOSAT* data, and a different quadratic pulse phase model for each outburst in the BATSE or *RXTE* PCA data. Table 2 (fifth row) lists the orbital parameters for the combined fit. Figure 2 shows the phase residuals (top panel) from BATSE and *RXTE* and frequency residuals (bottom panel) from *EXOSAT* for this fit.

Figure 3 shows the intrinsic pulse frequencies from the outbursts observed with *EXOSAT*, barycentered and corrected for the orbit from the combined fit. The bottom panel shows the spin-up rate computed by differencing adjacent pulse frequencies. The pulse frequency measurement on 1985 October 29 (MJD 46367) was omitted because it had a large measurement error due to the short  $< 3000$  second observation. At the end of the giant outburst and in between the outbursts, the pulse frequencies are consistent with a constant value. During the second outburst, the average frequency derivative was  $(9.7 \pm 3.9) \times 10^{-13}$  Hz  $s^{-1}$ , suggesting mild spin-up, similar to many of the weaker outbursts observed with BATSE and *RXTE*. The spin-up rate during the giant outburst is now consistent with a smooth trend. The improved orbital parameters derived from the joint fit to *EXOSAT*, BATSE, and *RXTE* data have removed the temporary enhanced spin-up reported by Reynolds et al. (1996).

Figure 4 shows the long-term history of the spin frequency of EXO 2030+375, barycentered and corrected using the orbit from this joint fit. This history includes spin frequency measurements from the *EXOSAT*, BATSE, and *RXTE* data used in our orbital fits. In addition, the pub-

lished pulse frequency measurement from 1989 *Ginga* observations (Sun et al. 1992) is shown and has been corrected using our improved orbital parameters. The *Ginga* observations were not used in our orbital analysis because they spanned less than 3 days, which was too short to extract additional orbital information. During the initial giant outburst observed with *EXOSAT*, EXO 2030+375 spun-up at an average rate of  $(1.1 \pm 0.1) \times 10^{-11}$  Hz  $s^{-1}$ . Between the second outburst observed with *EXOSAT* and the first outburst observed with BATSE, the average spin-up rate was two orders of magnitude smaller than in the giant outburst, but still substantial at  $(1.37 \pm 0.07) \times 10^{-13}$  Hz  $s^{-1}$ . During the BATSE era, EXO 2030+375 exhibited both spin-up and spin-down. From *CGR0* launch until about 1992 February (MJD 48660), EXO 2030+375 was consistent with a constant spin frequency. For about 1.8 years from 1992 February until 1993 November (MJD 48660-49308), the average spin-up rate was  $(1.91 \pm 0.04) \times 10^{-13}$  Hz  $s^{-1}$ , during the brighter outbursts observed with BATSE. When the outbursts became fainter, EXO 2030+375 began to spin down at an average rate of  $(-5.3 \pm 0.1) \times 10^{-14}$  Hz  $s^{-1}$ , for the last  $\sim 6.5$  years of the BATSE mission. The average spin-up rates suggest that EXO 2030+375's spin history was different during the intervening period between *EXOSAT* and BATSE observations than during the BATSE era. Between the last *EXOSAT* and first BATSE observation, separated by about 5.5 years, there is significant average spin-up, suggesting that the pulsar was spinning-up for a significant fraction of the time. In contrast, the average spin-up rate during the first 5.5 years of the BATSE mission was a factor of  $\sim 2$  smaller. Another giant outburst with a frequency change equal to that in the *EXOSAT* outburst was probably not missed. If one occurred just after the second outburst observed with *EXOSAT*, a spin-down rate of  $\gtrsim 4$  times that observed with BATSE would be needed to spin the pulsar down to the spin frequency observed with BATSE. Interpretation of source behavior based on average spin-up rates needs to be treated with caution. Comparing only the spin frequencies from the first and last BATSE observation, to mimic the sparse observations prior to the BATSE era, one would erroneously conclude that EXO 2030+375 had remained at an approximately constant spin

frequency over 9 years, which is clearly not the case.

### 2.3. Spin-up Torque vs. Flux correlations

If an accretion disk is present in an accreting pulsar system, we expect to see a correlation between spin-up and flux based on accretion theory. In the giant outburst observed with *EXOSAT* such a correlation was observed (Parmar et al. 1989; Reynolds et al. 1996; Stollberg et al. 1999). The detection of a QPO at 0.2 Hz by Angelini, Stella, & Parmar (1989) provided further evidence of an accretion disk. However, previous studies (Stollberg et al. 1999) were unable to determine if such a correlation was also present in the BATSE data due to coupling between the torque model and orbital parameters. Since we now have a good orbital solution that is not strongly coupled to the assumed torque model, we can address whether or not the spin-up rate is correlated with flux in the BATSE observations. Here we first consider the BATSE data, then revisit *EXOSAT* data, and lastly estimate a bolometric correction to compare them.

For each outburst observed with BATSE, we fitted the one day pulse phase measurements with corresponding barycentered and orbit corrected arrival times using a quadratic phase model. This model gave us the average spin-up rate for each outburst. We averaged the 1-day pulsed flux measurements for each outburst to get the average 20-50 keV pulsed flux. Figure 5 (left panel) is a linear plot of the BATSE spin-up rates versus 20-50 keV pulsed flux. The BATSE spin-up rates are correlated with the BATSE pulsed fluxes, with a linear correlation coefficient of 0.85 with a chance probability of  $10^{-4}$ . We fitted the data with a power-law (dotted line in the left panel of Figure 5), obtaining an index of  $2.2 \pm 0.6$ , although the fit was formally unacceptable. We also fitted the BATSE data with a linear model. The best-fit line to the BATSE data (solid line in Figure 5) had a slope of  $(5.0 \pm 1.0) \times 10^{-3} \text{ Hz erg}^{-1} \text{ cm}^2$  and an x-intercept (20-50 keV pulsed flux at zero spin-up) of  $(1.5 \pm 0.3) \times 10^{-10} \text{ ergs cm}^{-2} \text{ s}^{-1}$ .

Figure 5, right-hand panel, shows the spin-up rates divided by the 1-20 keV flux versus the 1-20 keV flux from *EXOSAT* observations. These units are chosen to better illustrate deviations from simple power law and the Ghosh & Lamb (1979) mod-

els than a log-log plot of spin-up rate versus flux. Spin-up rates (shown in Figure 3), were computed by differencing adjacent spin frequencies measured using our improved orbital parameters. Fluxes in the 1-20 keV band were computed from the luminosities in Table 1 in Parmar et al. (1989). The 1-20 keV flux corresponding to each spin-up rate was computed by averaging adjacent fluxes. We fitted the *EXOSAT* data with a power law (dotted line in right panel of Figure 5), obtaining an index of  $1.17 \pm 0.04$  (denoted by a dotted line), although the fit was formally unacceptable. Previous fits to these data using different orbital solutions gave power law slopes of 1.1-1.4 (Parmar et al. 1989), 1.2 (Reynolds et al. 1996), and  $1.02 \pm 0.12$  (Stollberg et al. 1999), although all of these fits were also formally unacceptable. In the right-hand panel of Figure 5, a dashed line denotes our best-fit power law with an index fixed at 6/7 which represents the relationship between spin-up and flux predicted by simple accretion theory. We have also overlaid Reynolds et al. (1996)'s fit of the Ghosh & Lamb (1979) model as a dot-dashed line. (See Reynolds et al. 1996 for the model formulation and parameters).

To compare the BATSE and *EXOSAT* data, we computed an approximate bolometric correction using the faint 1996 July outburst which was observed by both BATSE and *RXTE*. The average 20-50 keV pulsed flux for MJD 50266-50274 (1996 July 2-10) was  $1.18 \times 10^{-10} \text{ ergs cm}^{-2} \text{ s}^{-1}$  and the average 2.7-30 keV flux measured with *RXTE* for those dates was  $9.47 \times 10^{-10} \text{ ergs cm}^{-2} \text{ s}^{-1}$  (Reig & Coe 1999). Taking the ratio of the two fluxes gives a bolometric correction of  $\sim 8.0$  for the BATSE data. Several sources of systematic error affect this correction including differences in energy calibrations of BATSE, *RXTE*, and *EXOSAT*, and variations of the spectrum and pulse fraction with luminosity. Because of these systematic errors, the comparison of the two data sets can only be qualitative. The solid box in the right panel of Figure 5 denotes the linear fit to the BATSE data projected on to this plot by assuming a range of bolometric corrections from 5.6-10.4, i.e., our estimated correction with an assumed systematic error of 30%.

### 2.4. X-ray Flux Measurements

BATSE provided nearly continuous monitoring of the whole sky in the 20 keV to 2 MeV band us-



ing the Earth occultation technique (Wilson et al. 2000; Harmon et al. 2001). When a source went behind (or emerges from behind) the Earth, step-like features were produced in the BATSE data twice every 90 minute orbit. To measure the intensity of a known source, about 2 minutes of data (in each of 16 energy channels and each detector, using the 2.048 s CONT data) immediately before and after the occultation step were fitted with a model consisting of a quadratic background plus source terms for the source of interest and any interfering sources within  $70^\circ$  of the detector normal. Unfortunately, in the case of EXO 2030+375, the bright, highly variable sources Cyg X-1 and Cyg X-3 produce systematic errors in the step measurements. When these sources were not Earth occulted, they could produce rapid variations in the total count rate which could cause the size of the EXO 2030+375's steps to be under or overestimated. Variations in the bright source could also produce a positive or negative offset in the average step measurement (See Harmon et al. 2001 for a detailed description of systematic errors). The strength of these systematic errors varied with both the brightness of the sources and the 52-day precession period of the spacecraft. To attempt to address these systematic errors, we epoch-folded rising and setting occultation steps separately for MJD 48363-49535 (1991 Apr- 1993 Dec) when EXO 2030+375 was brighter, shown in the top and center panels, respectively, of Figure 6. Since rising and setting steps sampled different slices of the sky, features present in both plots are likely due to EXO 2030+375. However, the setting steps were less contaminated by Cygnus X-1 than the rising steps because Cygnus X-1 always rose before EXO 2030+375, hence it always affected the rising step measurements, but Cygnus X-1 also always set before EXO 2030+375. The setting steps from Cygnus X-1 were still within the fitting window for EXO 2030+375, but since Cygnus X-1 was active for less of the fitting window than in the rising steps, it had a smaller effect. Evidence of these systematic effects can be seen by comparing the minima in the top and center panels of Figure 6. Systematic effects caused the minimum to be offset from zero by a negative value. In the top panel, the minimum is about twice as negative as in the center panel, suggesting more interference. In both panels, there is a

suggestion of emission near apastron. Further possible evidence for apastron emission is shown in Figure 7 which shows Lomb-Scargle periodograms for the rising (top panel) and setting (bottom panel) occultations from MJD 48363-49353 (1991 Apr - 1993 Dec). In both periodograms, there are significant peaks at the EXO 2030+375 orbital period  $P_{\text{orb}}$  (chance probabilities  $8.1 \times 10^{-12}$  and  $3.6 \times 10^{-16}$  for the top and bottom panels, respectively) and at  $P_{\text{orb}}/2$  (chance probabilities  $7.2 \times 10^{-5}$  and  $5.3 \times 10^{-4}$  for the top and bottom panels, respectively). The chance probabilities and confidence levels (listed in the caption to Figure 7) were computed using a Monte-Carlo simulation to generate the probability distribution for the null hypothesis over the frequency range  $0.005 - 0.01 \text{ d}^{-1}$  and then fitting Equation 13.8.7 from (Press et al. 1992) by least squares. These peaks are consistent with a double-peaked orbital light curve. Reig et al. (1998) reported  $\sim 3\sigma$  evidence for apastron emission in *RXTE* ASM data from a later epoch, 1996-1998 February (MJD 50135-50870). To look for additional evidence of apastron outbursts, we epoch-folded the available *RXTE* ASM 1-dwell data, using a period of 46.0214 days and a periastron epoch of MJD 50547.22. Figure 6 (bottom panel) shows the folded profile from MJD 50135-52138 (1996 February - 2001 August). Filled squares denote points that are  $> 5\sigma$  above the  $0.075 \text{ counts sec}^{-1}$  (1 mCrab) positive bias found in long-term averages of ASM data according to the ASM Instrument Team and apparent in the sum band light curves of sources believed to be well below the ASM threshold (e.g., SS 0019+21, X 0620-003, and PSR J1022+1001). This ASM folded profile shows  $5.2\sigma$  evidence for apastron emission.

Because EXO 2030+375 is brighter in the 2-10 keV band than in BATSE's 20-50 keV band, the *RXTE* ASM more easily detects individual outbursts of EXO 2030+375. Figure 8 shows the 2-10 keV flux history for EXO 2030+375 measured with the *RXTE* ASM. The ASM routinely scans the sky with  $\sim 90$  second "dwells" on each sky region. We averaged the "dwells" over 4-day intervals to improve our sensitivity to EXO 2030+375 outbursts. Filled circles in Figure 8 denote 4-day averages that are  $\gtrsim 3\sigma$  measurements. The majority of the apparent detections are near the time of periastron passage denoted with dotted

vertical lines. In fact, for the 43 periastron passages observed as of 2001 August with the *RXTE* ASM, since MJD 50135 (1996 February 21), only 2 fail to show  $\gtrsim 3\sigma$  evidence of an outburst. The *RXTE* ASM saw evidence for an outburst in all but one of the cases where no outburst was detected with BATSE (See Table 1) in the period when both instruments were active. Prior to the launch of *RXTE*, BATSE occasionally failed to detect an outburst near EXO 2030+375's periastron passages, with the most consecutive missed outbursts being 3 outbursts from MJD 49867-50032 (1995 May 30 - Nov 11). Combining the *RXTE* and BATSE results, we find that EXO 2030+375 appears to have undergone an outburst every periastron passage for 82 periastron passages from 1991 April to 2001 August (MJD 48361 - 52138). For the 11 periastron passages where no outburst was detected (9 prior to the launch of *RXTE*), EXO 2030+375 most likely still had an outburst that peaked just below our detection threshold.

To investigate the orbital phasing of the outbursts, we determined the time of outburst peaks by fitting a Gaussian to the 1-day BATSE 20-50 keV pulsed flux measurements described in Section 2.2 for each outburst. In addition, for each predicted periastron passage where *RXTE* ASM data were available, we fitted a Gaussian to 46.0214 days of single dwell 2-10 keV flux measurements centered on the predicted periastron time. Figure 9 shows the orbital phase of the outbursts versus time. Dashed lines indicate the intervals of orbital phase where pulsations were detected with BATSE. Arrows indicate the orbital phase range of outbursts where pulsations were detected with the *RXTE* PCA, the second of which was not detected with BATSE. Filled squares indicate the time of outburst peaks determined from BATSE pulsed fluxes and open circles indicate peaks determined from ASM data. If the error on the Gaussian centroid was larger than 5 days, that point was not plotted. From MJD 48361-49900 (1991 Apr - 1995 Jul), the outbursts occurred at a stable orbital phase, peaking about 6 days after periastron passage. Three outbursts were not detected with BATSE following this interval, but when the outbursts were again detected after MJD 50000 (1995 Oct 10), they peaked about 4 days before periastron passage. The orbital phase of these outbursts slowly recovered to about 2.5 days after

periastron.

## 2.5. Optical/IR Observations

Infrared observations were obtained using the Continuously Variable Filter Photometer on the 1.5m Carlos Sanchez Telescope at the Teide Observatory, Tenerife, Spain as part of the Southampton-Valencia monitoring campaign. Figure 10 shows long-term infrared photometric measurements of the optical counterpart to EXO 2030+375. Observations prior to MJD 49929 (1995 Jul 31) are taken from Table 2 in Reig et al. (1998). For isolated Be stars, variations in these bands are believed to be good indicators of the size of the Be star's equatorial disk. However, when the Be star is in a binary system with a neutron star, the Be disk is truncated at a resonance radius by tidal forces from the orbit of the neutron star (Okazaki & Negueruela 2001). In these cases, as the disk cannot easily change size because of the truncation radius, changes in mass loss from the Be star produce changes in the disk density, which can even become optically thick at IR wavelengths. In this case, the IR magnitudes and the  $H\alpha$  equivalent width are more related to the disk density than to the disk radius (Negueruela et al. 2001; Miroshnichenko et al. 2001, for example). Although there was a gap with no measurements from MJD 47106-48565 (1987 Nov - 1991 Nov), the magnitudes in all three bands remained at the same level from near the end of the giant outburst observed with *EXOSAT* until about MJD 49000 (1993 Jan). From MJD 49000 until it reached a minimum near MJD 50300 (1996 Aug), the magnitudes in all 3 bands slowly became fainter, indicating a declining density in the Be disk. The Be star apparently did not go into a disk-loss phase as has been observed in other systems (e.g., A0535+262, Negueruela et al. 2000). Instead, the IR measurements indicate that the density of the disk began to increase.

One of the best direct tools for determining if there have been any major structural changes in the circumstellar disk around the Be star is the profile of the  $H\alpha$  line. Presented in Figure 11 are a sample of such profiles covering the period of interest; the details of the observations are presented in Table 3. The equivalent widths (EW) of most of the observations have been published in Reig et al. (1998). In this paper we are primarily

concerned with the shapes of the  $H\alpha$  profiles, none of which have previously been published.

Looking at the 1997 and 1998 spectra one can see definite evidence that the profile is not just a simple one, even though the signal to noise ratio is rather lower than the earlier brighter spectra. The extended nature of the profiles is indicative of a significantly different circumstellar disk structure than before. Certainly the well established correlation between the  $H\alpha$  EW and the IR flux for this source Reig et al. (1998) enables one to use the IR flux as an excellent indicator that changes were taking place around this time in the disk.

Because of the weak flux in the profiles it is not possible to say anything definite about the shapes of the profiles, but they appear similar to the double structures seen in many such systems. Certainly the 1997 and 1998 profiles are much wider than the 1996 one (all observed at similar resolutions with the same telescope), indicating the presence of material in the circumstellar disk moving at high velocities close to the Be star. This could well be direct evidence for the re-building of the disk after the extended low period.

Parmar et al. (1989) estimated a distance of 5 kpc to EXO 2030+375 and the fitted values from torque models in Reynolds et al. (1996) are also in that range. However, optical data require a larger distance. Coe et al. (1988) determined an interstellar extinction of  $E(B - V) = 3.74$  from optical photometry which agreed well with the X-ray column density determined with *EXOSAT*. Since EXO 2030+375 is within  $1.5^\circ$  of the galactic plane, we use the relationship between extinction and distance for objects in the plane (Binney & Merrifield 1998) and get  $d = 7.1 \pm 0.2$  kpc (assuming an error of  $\sim 0.1$  on the interstellar extinction).

### 3. Discussion

#### 3.1. Improvements to Sensitivity and Orbital Parameters

Improvements to our techniques used to search for pulsations in the BATSE data reduced systematic errors to below statistical levels. These improvements included using a modified  $Z_n^2$  statistic which accounted for aperiodic noise from either the measured source or others in the field of view such as Cygnus X-1 and automatically fitting Earth occultation steps from bright sources using

a database including source locations, dates of activity, and flux levels to determine which sources needed to be fitted. These improvements allowed us to use much longer integrations for searches, e.g. 4 days, with accurately determined errors. Searches of BATSE data using these new techniques resulted in detection of 52 outbursts including several in the 2.5 year period from 1993 August to 1996 April when EXO 2030+375 was previously believed to be quiescent. Our results show that EXO 2030+375 has undergone an outburst near most likely every periastron passage for 9 years. From MJD 50643-51004 (1997 Jul - 1998 Jul), EXO 2030+375 went undetected with BATSE for the longest interval, 7 periastron passages. However, *RXTE* PCA observations detected an outburst from EXO 2030+375 on the third periastron passage missed with BATSE and the *RXTE* ASM detected outbursts for 6 of those periastron passages, suggesting that outbursts were still occurring but were below BATSE's detection threshold. Cygnus X-1 was noisy during this time interval. Additional noise plus a slight decrease in the intensity of EXO 2030+375 likely explains why BATSE missed these outbursts.

The 13 consecutive outbursts used by Stollberg et al. (1999) to determine an orbit for EXO 2030+375 provided good coverage from periastron passage to about 14 days after periastron passage. Their orbit fitting was further complicated by the intrinsic spin frequency variations during these 13 brighter outbursts. Comparing panel (b) in Figure 1 and Figure 9 shows where there were problems with the Stollberg et al. (1999) orbital parameters. The outbursts from MJD 50000-50700 (1995 Oct - 1997 Sep) covered earlier orbital phases, from about 7.5 days before until 6 days after periastron passage, than those included in the orbit fitting of Stollberg et al. (1999). These outbursts showed excess scatter in the spin frequencies determined using the orbital parameters of Stollberg et al. (1999), indicating that fitting those outbursts would improve the orbital parameters. Fits to BATSE and *RXTE* data from these outbursts in addition to the outbursts fitted by Stollberg et al. (1999) resulted in improved orbital parameters that removed the excess scatter in the spin frequencies. The orbital parameters were further improved by including pulse frequencies determined from *EXOSAT* ME data during the initial giant

outburst, which provided coverage of the entire orbit including two periastron passages with good coverage of orbital phases from 21 to 7 days before periastron passage. Fits to a broad range of orbital phases allowed us to decouple orbital and intrinsic effects and to provide a good determination of the orbital parameters without using complicated models for the intrinsic torque variations. Our new orbital parameters are given in Table 2.

### 3.2. Orbital Phasing of Outbursts

The outbursts prior to MJD 50000 (1995 Oct) peaked at a very regular orbital phase of about 6 days after periastron passage (see Figure 9). The outburst just after MJD 50000 peaked at a much earlier orbital phase, 4 days before periastron passage and then gradually recovered to peak at a new stable orbital phase of about 2.5 days after periastron passage. A possible explanation of the shift in orbital phase of the outbursts is a density perturbation (global one armed oscillation) in the Be disk. Evidence for these density perturbations is seen in the  $H\alpha$  line profiles for several Be/X-ray binaries (Negueruela et al. 2001; Negueruela & Okazaki 2001, for example). When a density perturbation is present, the  $H\alpha$  line is double peaked. The relative size of the two peaks changes with a cycle of several years. The density perturbation produces a non-axially symmetric Be disk. If the pulsar interacts with a region of the disk affected by the perturbation, more material would be available for accretion, possibly causing a shift in outburst phase. The trend in the orbital phases from MJD 50000-50600 (1995 Oct - 1997 Jun) in Figure 9 has a slope of  $m = 0.0085 \pm 0.0017$ . This slope can be expressed in terms of a beat frequency between the orbital period and some other period. Assuming the other period is longer than the orbital period, as is expected for global one-armed oscillations, then

$$m = \frac{\nu_{\text{beat}}}{\nu_{\text{orb}}} - 1 \quad (2)$$

where  $\nu_{\text{beat}}$  is the beat frequency and  $\nu_{\text{orb}}$  is the orbital frequency. If this trend is due to beating between the orbital period and the period of the density perturbation, then the beat frequency of is given by

$$\nu_{\text{beat}} = \nu_{\text{orb}} + \nu_{\text{perturb}} \quad (3)$$

where  $\nu_{\text{perturb}}$  is the frequency of the density perturbation. Solving for  $\nu_{\text{perturb}}$ , we get a perturbation frequency of  $(1.8 \pm 0.4) \times 10^{-4}$  cycles day $^{-1}$  or equivalently, a period of  $15 \pm 3$  years for the density perturbation to propagate around the Be disk. No significant change in X-ray intensity was seen when the outbursts shifted in orbital phase, although 3 outbursts went undetected near the time when the shift occurred. *EXOSAT* observations of the second outburst of EXO 2030+375 after its discovery (1985 October 29–November 3, MJD 46367–46372) show that the outburst peaked at  $9.5 \pm 1.1$  days after periastron, assuming that the peak flux detected with *EXOSAT* is the peak of a normal outburst. Interestingly, this is 3.5 days later than the peak time observed in the pre-MJD 50000 (1995 Oct) BATSE data, which is also 3.5 days later than the peak time observed after MJD 51000 (1998 Jul), when the peak time had stopped changing rapidly and occurred about 2.5 days after periastron. This suggests that another shift in outburst phase may have occurred between the *EXOSAT* and BATSE observations. However, if such a shift occurred, it suggests a shorter propagation period of  $\lesssim 10$  years.

Optical observations of the  $H\alpha$  profile (Figure 11) clearly indicate that the structure of the circumstellar disk around the Be star changed significantly at some time between the 1996 July (MJD 50273) observation and the 1997 August (MJD 50661) observation. These observations support the idea of a global one-armed oscillation propagating in the Be disk suggested by the shift in orbital phase of the outbursts. However, sparse observations of the  $H\alpha$  profile do not allow us to directly correlate  $H\alpha$  profile changes with changes in the X-ray outbursts.

### 3.3. Relationship between X-ray and IR Measurements

Comparing the IR measurements in Figure 10 to the X-ray measurements (Figures 1 and 4) suggests a relationship between the IR behavior and the X-ray activity. The IR measurements indicate that the Be disk was fairly stable and roughly constant in density from near the end of the initial giant outburst until MJD 49000 (1993 Jan). Figure 4 indicates that the pulsar was spinning up for most of this period. Near MJD 49000, the density of the disk began to decline. Since the disk

was becoming less dense, the reservoir of material available to the pulsar near periastron passage was slowly reduced. After MJD 49250 (1993 Sep), the X-ray pulsed flux responded to the lower density disk and dropped dramatically. Peak 20-50 keV pulsed fluxes dropped from  $(3 - 5) \times 10^{-10}$  ergs  $\text{cm}^{-2} \text{s}^{-1}$  to  $\lesssim 1.5 \times 10^{-10}$  ergs  $\text{cm}^{-2} \text{s}^{-1}$ . The global spin-up rate of the pulsar took longer to respond. After about MJD 49250, the spin-up rate slowed and by MJD 49400 (1994 Feb), the pulsar had begun to spin-down. No obvious response in the X-rays was seen to the slow increase in density of the Be disk indicated by the IR measurements after MJD 50300 (1996 Aug). Perhaps the disk had not yet become dense enough to increase the mass accretion rate to a level where the pulsar would begin to spin-up.

To determine whether or not the observed spin-down was likely due to centrifugal inhibition of accretion (Stella, White, & Rosner 1986), i.e., the propeller effect (Illarionov & Sunyaev 1975), we estimate the flux at the onset of this effect by equating the magnetospheric radius to the corotation radius. The magnetospheric radius is given by (Pringle & Rees 1972; Lamb, Pethick, & Pines 1973)

$$r_m \simeq k(GM)^{1/7} \mu^{-2/7} L^{-2/7} R^{-2/7} \quad (4)$$

where  $G$  is the gravitational constant;  $M$  and  $R$  are the mass and radius of the neutron star; and  $L$  is the luminosity.  $k$  is a constant factor of order 1. Equation 4 with  $k \simeq 0.91$  gives the Alfvén radius for spherical accretion and with  $k \simeq 0.47$  gives the magnetospheric radius derived by Ghosh & Lamb (1979). The corotation radius is given by

$$r_{co} = (GM)^{1/3} (2\pi\nu)^{-2/3} \quad (5)$$

where  $\nu$  is the spin frequency of the pulsar. Setting  $r_m = r_{co}$  gives the threshold flux for the onset of centrifugal inhibition of accretion, i.e.,

$$F_x^{\min} \simeq 3 \times 10^{-10} \text{ ergs cm}^{-2} \text{ s}^{-1} k^{7/2} \mu_{30}^2 M_{1.4}^{-2/3} R_6^{-1} P_{41.7s}^{-7/3} d_{\text{kpc}}^{-2} \quad (6)$$

where  $\mu_{30}$ ,  $M_{1.4}$ ,  $R_6$ , and  $P_{41.7s}$  are the pulsar's magnetic moment in units of  $10^{30}$  G  $\text{cm}^3$ , mass in units of  $1.4 M_\odot$ , radius in units of  $10^6$  cm, and spin period in units of 41.7 seconds, respectively. Reynolds et al. (1996) fitted 3 accretion torque models, a simple spherical accretion model, the Ghosh & Lamb (1979) model, and the Wang

(1987) model to the giant outburst to estimate values for  $\mu_{30}$  and  $d_{\text{kpc}}$ . For the simple spherical accretion model, where  $k \simeq 0.91$ , Reynolds et al. (1996) obtained  $\mu_{30} \simeq 5$  for an assumed distance of  $d_{\text{kpc}} = 5$ . Both the Ghosh & Lamb (1979) model and the Wang (1987) model use  $k \simeq 0.47$ . Reynolds et al. (1996) obtained  $\mu_{30} \simeq 12$  and  $d_{\text{kpc}} \simeq 5.2$  from fits to the (Ghosh & Lamb 1979) model. Parmar et al. (1989) also fitted the Ghosh & Lamb (1979) model, obtaining  $\mu_{30} \simeq 20$  and  $d_{\text{kpc}} \simeq 5.3$  for the first nine period measurements and  $\mu_{30} \simeq 11$  and  $d_{\text{kpc}} \simeq 5.0$  for the first 10 period measurements. Reynolds et al. (1996) fit of the Wang (1987) model yielded the lowest distance  $d_{\text{kpc}} \simeq 4.1$  with  $\mu_{30} \simeq 10$ . Substituting Reynolds et al. (1996) values yields  $F_x^{\min} \simeq (1.1 - 2.2) \times 10^{-10}$  ergs  $\text{cm}^{-2} \text{s}^{-1}$  while Parmar et al. (1989)'s values yield  $F_x^{\min} \simeq (1 - 3) \times 10^{-10}$  ergs  $\text{cm}^{-2} \text{s}^{-1}$ .

The minimum flux where pulsations were first detected during the faint 1996 July outburst observed with *RXTE* was  $3.3 \times 10^{-10}$  ergs  $\text{cm}^{-2} \text{s}^{-1}$  (Reig & Coe 1999, 2.7-30 keV), which is comparable to the lowest flux of  $4 \times 10^{-10}$  ergs  $\text{cm}^{-2} \text{s}^{-1}$  observed by Parmar et al. (1989) before pulsations became undetectable in the giant outburst. Since pulsations were detected with *RXTE* and no significant changes in the 2-10 keV pulse profile were observed relative to higher fluxes (Reig & Coe 1998), this flux is most likely above the threshold for centrifugal inhibition of accretion, which is consistent with our calculations in the previous paragraph. On 1985 August 25, when pulsations were not detected, Parmar et al. (1989) measured an upper limit of  $1.3 \times 10^{-11}$  ergs  $\text{cm}^{-2} \text{s}^{-1}$  on the flux from EXO 2030+375, which places a lower bound on  $F_x^{\min}$ , that is also consistent with our calculations, assuming that the observed sudden drop in flux was due to centrifugal inhibition of accretion.

### 3.4. Spin-up vs. flux correlations

In giant outbursts of Be/X-ray binaries, accretion disks are expected to be present and indeed, evidence for an accretion disk, based on a correlation between the observed flux and spin-up rate, has been found for several sources including EXO 2030+375 (Parmar et al. 1989; Reynolds et al. 1996; Stollberg et al. 1999) during giant outbursts of Be/X-ray binaries (Wilson et al. 1998;

Bildsten et al. 1997). Independent evidence for an accretion disk based on the detection of quasi-periodic oscillations during a giant outburst has been found for EXO 2030+375 (Angelini, Stella, & Parmar 1989) and A0535+262 (Finger, Wilson, & Harmon 1996). In addition to the expected correlation between observed flux and spin-up rate in the giant outburst of EXO 2030+375, the BATSE data suggest a correlation is also present in the brighter normal outbursts of this system (See Figure 5). Until recently, normal outbursts were believed to be due to direct wind accretion from the Be disk, so significant spin-up was not expected because wind accretion is not believed to be very efficient at transferring angular momentum (Ruffert 1997). However, evidence for spin-up during normal outbursts has been observed in GS 0834–430 (Wilson et al. 1997), 2S 1417–624 (Finger, Wilson, & Chakrabarty 1996), 2S 1845–024 (Finger et al. 1999), and previously in EXO 2030+375 (Stollberg et al. 1999). In BATSE observations of 2S 1845–024, a correlation between the spin-up rate and the pulsed flux was also observed.

The comparison of the BATSE and EXOSAT data in Figure 5, despite an uncertain bolometric correction, shows that at the lower fluxes measured with BATSE the correlation falls off more rapidly than a power law. This suggests either that spin-down torques become important or perhaps that a disk forms during the outburst and we are averaging over periods of wind and disk accretion. The data are clearly inconsistent with the power law index of 6/7 predicted from simple accretion theory, which does not consider spin-down torques. The Ghosh & Lamb (1979) model fitted by Reynolds et al. (1996), which assumes an accretion disk is present, roughly follows the trend observed in the data; however, the brightest *EXOSAT* observations, which drive the fit, clearly deviate from the model. The observed flux is given by  $F = (\beta L)/(4\pi d^2)$ , where  $\beta$  is a beaming factor. This beaming factor, which is typically assumed to be equal to one for simplicity, depends on the pattern of emitted radiation at the pulsar and cannot be determined without modeling of the pulse profiles (which is beyond the scope of this work). Because large luminosity dependent 1–10 keV pulse profile variations were observed during the giant outburst (Parmar, White, & Stella 1989), one would expect that the beaming factor

was also changing with luminosity. To fit any of the discussed models, the beaming factor must decrease with increasing luminosity.

The spin-up rate and its correlation with pulsed flux during the earlier outbursts of EXO 2030+375 observed with BATSE suggest an accretion disk may be present. A disk will form if the specific angular momentum of the material accreted from the Be star’s disk is comparable to the Keplerian specific angular momentum at the magnetospheric radius. The specific angular momentum  $\ell$  of the accreted material is given by

$$\ell = 2\pi I \dot{\nu} \dot{M}^{-1} \simeq (4.8 - 9.1) \times 10^{16} \text{ cm s}^{-1} d_{7.1\text{kpc}}^{-2}, \quad (7)$$

assuming  $\dot{M} = L(GM/R)^{-1}$ . Here  $\dot{\nu} = 6.5 \times 10^{-13} \text{ Hz s}^{-1}$  is the spin-up rate,  $\dot{M}$  is the mass accretion rate,  $L = (0.8 - 1.6) \times 10^{37} \text{ ergs s}^{-1} d_{7.1\text{kpc}}^2$  is the luminosity, and  $d_{7.1\text{kpc}}$  is the distance in units of 7.1 kiloparsecs. The spin-up rate and luminosity are outburst averaged values from a typical bright outburst observed with BATSE in 1992 February. The luminosity is estimated from BATSE pulsed flux of  $2.5 \times 10^{-10} \text{ ergs cm}^{-2} \text{ s}^{-1}$  using a bolometric correction of  $8.0 \pm 2.4$  (See Section 2.3), and a distance of 7.1 kpc (See Section 2.5). We have assumed typical pulsar parameters, listed in Section 3.3. If  $\ell \sim \ell_m = (GM r_m)^{1/2}$ , the Keplerian specific angular momentum at the magnetospheric radius, a disk will form. Once a disk has formed the specific angular momentum of accreting material is maintained near  $\ell_m$ . At  $F_x^{\text{min}}$  (Equation 6),  $r_m = r_{\text{co}}$ . Hence  $\ell_m$  can be expressed as a function of  $F_x^{\text{min}}$  and  $r_{\text{co}}$ , which is independent of the distance and magnetic field of the pulsar.

$$\ell_m \simeq 6.1 \times 10^{17} \text{ cm}^2 \text{ s}^{-1} P_{41.7\text{s}}^{1/3} \left( \frac{F}{F_x^{\text{min}}} \right)^{-1/7} \quad (8)$$

In the previous section, using *RXTE* and *EXOSAT* observations, we determined  $1.3 \times 10^{-11} \text{ ergs cm}^{-2} \text{ s}^{-1} \lesssim F_x^{\text{min}} \lesssim 3.3 \times 10^{-10} \text{ ergs cm}^{-2} \text{ s}^{-1}$ . With the estimated average bolometric flux of  $(1.4 - 2.6) \times 10^{-9} \text{ ergs cm}^{-2} \text{ s}^{-1}$  from the 1992 February outburst used in Equation 7, this yields  $\ell_m \simeq (2.9 - 5.0) \times 10^{17} \text{ cm}^2 \text{ s}^{-1}$ , which is within an order of magnitude of  $\ell \simeq (4.8 - 9.1) \times 10^{16} \text{ cm}^2 \text{ s}^{-1}$ , suggesting a disk is likely present because considerable angular momentum is present in the system. If a disk forms during the outburst, our average values of  $\dot{\nu}$  and  $F$  used in these calculations would include periods of wind accretion and

periods of disk accretion, possibly explaining why  $\ell \simeq (0.1 - 0.3)\ell_m$  rather than being a larger fraction. In contrast, for the wind-fed system Vela X-1 where a disk is not expected to be present,  $\dot{\nu} \simeq 6 \times 10^{-14} \text{ Hz s}^{-1}$  (Inam & Baykal 2000),  $L \simeq 2 \times 10^{38} \text{ ergs s}^{-1}$ , and  $\mu \simeq 2.1 \times 10^{30} \text{ G cm}^3$  (Makishima et al. 1999) leading to  $\ell \simeq 3.5 \times 10^{14} \text{ cm}^2 \text{ s}^{-1}$  and  $\ell_m \simeq 2.2 \times 10^{17} \text{ cm}^2 \text{ s}^{-1}$ , i.e.,  $\ell \simeq 0.002\ell_m$ .

### 3.5. Current Models

Although the direct wind accretion model has difficulty explaining evidence for an accretion disk during normal outbursts, the viscous decretion disk model (Lee, Osaki, & Saio 1991; Porter 1999; Okazaki 2001) provides a natural explanation. In this model, the inner edge of the Be disk has a Keplerian velocity. Viscosity conducts material outwards, so that it moves in quasi-Keplerian orbits with low radial velocities. The radial outflow is subsonic for the orbital sizes of all Be/X-ray binaries with a known solution. This model successfully accounts for most observations of Be disks (Okazaki & Negueruela 2001). Negueruela et al. (2001) found that tidal interaction of the neutron star truncates the circumstellar Be disk. In the disk, truncation occurs when the outward viscous torque is less than the inward resonant torque which truncates the disk at a resonant radius. Because of the truncation, the Be disk cannot reach a steady state (Okazaki & Negueruela 2001). According to the modeling of Okazaki & Negueruela (2001), the Be disk in EXO 2030+375 is likely truncated at the 4:1 resonance radius, which is close to the radius of the critical lobe at periastron. If the truncation radius is close to or slightly beyond the critical lobe radius at periastron, material with high angular momentum will flow through the first Lagrangian point to the neutron star, making formation of a transient accretion disk likely (Okazaki & Negueruela 2001) in a normal outburst. Hence this model provides a reasonable explanation of the brighter outbursts.

We propose the following scenario to explain the IR and X-ray observations. The Be disk is truncated at a 4:1 resonance radius. Following Okazaki & Negueruela (2001), there should be an outburst at every periastron unless the circumstellar disk disappears. Around MJD 49000 (sometime in 1993), a major structural change occurred in the Be star's circumstellar disk. It became much

less dense, as shown by the change in IR magnitudes and the  $\text{H}\alpha$  equivalent width. Much less matter was available for accretion, and as a consequence, the X-ray flux dropped and the neutron star spin-up ended. At the same time, or shortly afterward, a density wave (or global one-armed oscillation) developed and began to precess, without interacting with the neutron star's orbit. Around MJD 50000 (late in 1995), the density perturbation interacted with the neutron star's orbit, at a phase corresponding to about 3 days prior to periastron passage, producing an X-ray outburst peaked at that phase. This implies that the precession of the density perturbation was prograde, in the same sense as the neutron star's orbital motion. Sometime after about MJD 50600 (mid-1997), the density perturbation lost contact with the neutron star's orbit, in a position symmetrical with respect to periastron, i.e., about 3 days after periastron. This ended the fast migration of the outburst peaks in orbital phase. Some slow migration may still be present in Figure 9, which may eventually lead to the previous value of 6 days after periastron, after a complete precession period of the perturbed disk.

This research has made use of data obtained from the High Energy Astrophysics Science Archive Research Center (HEASARC), provided by NASA's Goddard Space Flight Center (GSFC). *RXTE* ASM quick-look results were provided by the ASM/RXTE teams at MIT and at the GSFC SOF and GOF. We are grateful to the support staff of the Telescopio Carlos Sanchez and the Service Programme of the Isaac Newton Group for help obtaining much of the optical and IR data. The TCS is operated on the Teide Observatory by the Instituto de Astrofísica de Canarias. We thank an anonymous referee whose suggestions improved our paper.

### REFERENCES

- Angelini, L., Stella, L., & Parmar, A.N. 1989, *ApJ*, 346, 906
- Apparao, K. 1991, *ApJ*, 375, 701
- Apparao, K. 1994, *Space Sci. Rev.* 69, 255
- Arnaud, K.A. 1996, *Astronomical Data Analysis*

- Software and Systems V, eds. G. Jacoby & J. Barnes, ASP Conf. Series, 101, 17
- Bildsten, L. et al. 1997, ApJS, 113, 367
- Binney, J. & Merrifield, M. 1998, Galactic Astronomy, (Princeton:Princeton University Press), 137
- Buccheri, R. et al. 1983, A&A, 128, 245
- Coe, M.J., Longmore, A., Payne, B.J., & C.G. Hanson 1988, MNRAS, 232, 865
- Corbet, R.H.D. 1986, MNRAS, 220, 1047
- Crary, D.J. et al. 1996, A&AS, 120, 153
- de Korte, P.A.J. et al. 1981, Space Sci. Rev., 30, 495
- Finger, M. H. et al. 1999, ApJ, 517, 449
- Finger, M.H., Wilson, R.B. & Chakrabarty, D. 1996, A&AS, 120, 209
- Finger, M.H., Wilson, R.B., Harmon, B.A. 1996, ApJ, 459, 288
- Fishman, G. J. et al. 1989, in Proc. GRO Science Workshop, ed. W.N. Johnson (Greenbelt: NASA/GSFC), 2
- Ghosh, P. & Lamb, F.K. 1979, ApJ, 234, 296
- Harmon, B. A. et al. 1992, in Compton Observatory Science Workshop (NASA Conf. Publ. 3137), ed. C. R. Schrader, N. Gehrels, & B. Dennis (Washington: NASA), 69
- Harmon, B.A. et al. 2001, ApJS, in press
- Hanuschik, R.W. 1996, A&A, 308, 170
- Illarionov, A.F. & Sunyaev, R.A. 1975, A&A, 39, 185
- Inam, S.C. & Baykal, A. 2000, A&A, 353, 617
- Jahoda, K. et al. 1996, EUV, X-ray, and Gamma-Ray Instrumentation for Astronomy VII, SPIE Proc. 2808, ed. O.H.V. Sigmund & M.Gumm (Bellingham:SPIE), 59
- Janot-Pacheco, E., Motch, C., & Pakull, M.W. 1988, A&A, 202, 81
- Lamb, F.K., Shibazaki, N., Alpar, M.A., & Shaham, J. 1985, Nature, 317, 681
- Lamb, F.K., Pethick, C.J., & Pines, D. 1973, ApJ, 184, 271
- Leahy, D.A. et al. 1983, ApJ, 266,160
- Lee, U., Osaki, Y., & Saio, H. 1991, MNRAS, 250, 432
- Levine, A.M., Bradt, H., Cui, W., Jernigan, J.G., Morgan, E.H., Remillard, R., Shirey, R. E., & Smith, D.A. 1996, ApJ, 469, L33
- Makishima, K., Mihara, T., Nagase, F., Tanaka, Y. 1999, ApJ, 525, 978
- Mavromatakis, F. 1994, A&A, 285, 209
- Miroshnichenko, A.S. et al. 2001, A&A, 377, 485
- Motch, C. & Janot-Pacheco, E. 1987, A&A, 182, L55
- Negueruela, I. et al. 2001, A&A, 369, 117
- Negueruela, I., Reig, P., Finger, M.H., Roche,P. 2000, A&A, 356, 1003
- Negueruela, I. & Okazaki, A.T. 2001, A&A, 369, 108
- Norton, A.J. et al. 1994, MNRAS, 271, 981
- Okazaki, A.T. 2001, PASJ, 43, 75
- Okazaki, A.T. & Negueruela, I. 2001, A&A, 377, 161
- Ostriker, E.C. & Shu, F.H. 1995, ApJ, 447, 813
- Parmar, A.N., White, N.E., Stella, L., & Ferri, P. 1989, ApJ, 338, 359
- Parmar, A.N., White, N.E., & Stella, L. 1989, ApJ, 338, 373
- Peacock, A. et al. 1981, Space Sci. Rev., 30, 525
- Porter, J.M. 1999, A&A, 348, 512
- Press, W. H. et al. 1992, Numerical Recipes in Fortran, Second Edition, (New York: Cambridge University Press), 569
- Pringle, J.E., & Rees, M.J. 1972, A&A, 21, 1



- Quirrenbach, A. et al. 1997, *ApJ*, 479, 477
- Reig, P. & Coe, M.J. 1998, *MNRAS*, 294, 118
- Reig, P. & Coe, M.J. 1999, *MNRAS*, 302, 700
- Reig, P., Stevens, J.B., Coe, M.J., & Fabregat, J. 1998, *MNRAS*, 301, 42
- Reynolds, A.P. et al. 1996, *A&A*, 312, 872
- Reynolds, A.P., Parmar, A.N., & White, N.E. 1993, *ApJ*, 414, 302
- Rothschild, R.E. et al. 1998, *ApJ*, 496, 538
- Ruffert, N. 1997, *A&A*, 317, 793
- Slettebak, A. 1988, *PASP*, 100, 770
- Standish, E. M., Newhall, X. X., Williams, J. G., & Yeomans, D. K. 1992, Orbital ephemerides of the Sun, Moon, & Planets, in Explanatory Supplement to the Astronomical Almanac, ed. P. K. Seidelmann (Mill Valley: University Science Books), 279
- Stella, L., White, N.E., & Rosner, R. 1986, *ApJ*, 308, 669
- Stollberg, M.T. et al. 1994, in The Evolution of X-ray Binaries, eds. S.S. Holt & C.S. Day (New York: AIP), 255
- Stollberg, M.T., Wilson, R.B., Finger, M.H., & Prince, T.A. 1996, *IAU Circ.* 6413
- Stollberg, M.T. et al. 1999, *ApJ*, 512, 313
- Sun, X.-J. et al. 1992, in Frontiers of X-ray Astronomy, eds. Y. Tanaka & K. Koyama (Tokyo: Universal Academy Press), 95
- Sun, X.-J., Li, T.-P., Wu, M., & Cheng, L.-X. 1994, *A&A*, 289, 127
- Turner, M.J.L. et al. 1981, *Space Sci. Rev.*, 30, 512
- van der Klis, M., Jansen, F., van Paradijs, J., Lewin, W.H.G, Sztajno, M., & Trümper, J. 1987, *ApJ*, 313, L19
- Wang, Y-M. 1987, *A&A*, 183, 257
- Waters, L.B.F.M. & van Kerkwijk, M.H. 1989, *A&A*, 223, 196
- Wilson, C.A. et al. 1997, *ApJ*, 479, 388
- Wilson, C.A. et al. 1998, *ApJ*, 499, 820
- Wilson-Hodge, C.A. 1999, PhD Dissertation, University of Alabama in Huntsville
- Wilson, C.A. et al. 2000, in Astronomical Data Analysis Software and Systems IX, ASP Conf. Ser. 216, eds. N. Manset, C Veillet, D. Crabtree, (Chelsea: ASP), 587
- Wilson, C.A., Finger, M.H., Coe, M.J., & Laycock, S. 2001, in Gamma-Ray Astrophysics 2001, AIP Conf. Proc. 587, (Melville: AIP), 34

---

This 2-column preprint was prepared with the AAS L<sup>A</sup>T<sub>E</sub>X macros v5.0.

TABLE 1  
EXO 2030+375 OUTBURST DETECTIONS

Number <sup>a</sup>	Start Date (MJD)	End Date (MJD)	Start Date (Calendar)	Stop Date (Calendar)
...	46203	46303	1985 May 18	1985 Aug 26
...	46367	46373	1985 Oct 29	1985 Nov 4
...	47828	47830	1989 Oct 29	1989 Oct 31
1	48385	48395	1991 May 9	1991 May 19
2	48433	48439	1991 Jun 26	1991 Jul 2
3	48475	48487	1991 Aug 7	1991 Aug 19
4	48524	48531	1991 Sep 25	1991 Oct 2
5	48569	48583	1991 Nov 9	1991 Nov 23
7 <sup>d</sup>	48659	48673	1992 Feb 7	1992 Feb 21
8 <sup>d</sup>	48705	48718	1992 Mar 24	1992 Apr 6
9 <sup>d</sup>	48753	48764	1992 May 11	1992 May 22
10 <sup>d</sup>	48799	48807	1992 Jun 26	1992 Jul 4
11 <sup>d</sup>	48846	48858	1992 Aug 12	1992 Aug 24
12 <sup>d</sup>	48890	48906	1992 Sep 25	1992 Oct 11
13 <sup>d</sup>	48936	48950	1992 Nov 10	1992 Nov 24
14 <sup>d</sup>	48984	48994	1992 Dec 28	1993 Jan 7
15 <sup>d</sup>	49028	49042	1993 Feb 10	1993 Feb 24
16 <sup>d</sup>	49076	49088	1993 Mar 30	1993 Apr 11
17 <sup>d</sup>	49120	49137	1993 May 13	1993 May 30
18 <sup>d</sup>	49166	49182	1993 Jun 28	1993 Jul 14
19 <sup>d</sup>	49214	49228	1993 Aug 15	1993 Aug 29
20	49261	49271	1993 Oct 1	1993 Oct 11
21	49305	49314	1993 Nov 14	1993 Nov 23
22	49351	49362	1993 Dec 30	1994 Jan 10
23	49398	49407	1994 Feb 15	1994 Feb 24
25	49491	49498	1994 May 19	1994 May 26
26	49536	49543	1994 Jul 3	1994 Jul 10
28	49629	49636	1994 Oct 4	1994 Oct 11
30	49719	49726	1995 Jan 2	1995 Jan 9
33	49861	49866	1995 May 24	1995 May 29
37	50033	50041	1995 Nov 12	1995 Nov 20
38	50082	50089	1995 Dec 31	1996 Jan 7
39	50125	50135	1996 Feb 12	1996 Feb 22
40	50176	50183	1996 Apr 3	1996 Apr 10
41	50221	50228	1996 May 18	1996 May 25
42 <sup>e,f</sup>	50265	50275	1996 Jul 1	1996 Jul 11
43	50313	50318	1996 Aug 18	1996 Aug 23
44 <sup>g</sup>	50359	50367	1996 Oct 3	1996 Oct 11
45	50404	50412	1996 Nov 17	1996 Nov 25
46	50452	50458	1997 Jan 4	1997 Jan 10
47	50500	50504	1997 Feb 21	1997 Feb 25
48	50545	50553	1997 Apr 7	1997 Apr 15
49	50591	50599	1997 May 23	1997 May 31
50	50639	50642	1997 Jul 10	1997 Jul 13
51 <sup>g</sup>	50684	50692	1997 Aug 24	1997 Sep 1
52 <sup>g</sup>	50728	50735	1997 Oct 7	1997 Oct 14
54 <sup>e</sup>	50821	50828	1998 Jan 8	1998 Jan 15
55 <sup>g</sup>	50867	50876	1998 Feb 23	1998 Mar 4
56 <sup>g</sup>	50915	50919	1998 Apr 12	1998 Apr 16
57 <sup>g</sup>	50956	50963	1998 May 23	1998 May 30
58	51005	51017	1998 Jul 11	1998 Jul 23
59	51051	51056	1998 Aug 26	1998 Aug 31
60	51096	51102	1998 Oct 10	1998 Oct 16
61	51143	51152	1998 Nov 26	1998 Dec 5
62	51189	51197	1999 Jan 11	1999 Jan 19
63	51233	51241	1999 Feb 24	1999 Mar 4
64	51281	51292	1999 Apr 13	1999 Apr 24
65 <sup>g</sup>	51327	51339	1999 May 29	1999 Jun 10
66	51372	51380	1999 Jul 13	1999 Jul 21
67 <sup>g</sup>	51415	51428	1999 Aug 25	1999 Sep 7
68	51469	51474	1999 Oct 18	1999 Oct 23
69 <sup>g</sup>	51511	51515	1999 Nov 29	1999 Dec 3
70	51558	51567	2000 Jan 15	2000 Jan 24
71	51601	51612	2000 Feb 27	2000 Mar 9

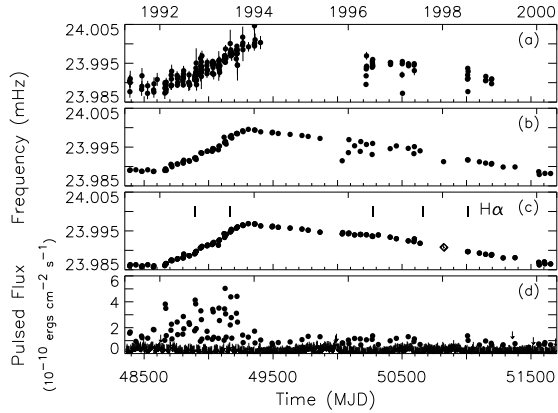


Fig. 1.— Panels (a)-(c): Comparison of the sensitivity of two different frequency search techniques and two orbital solutions using BATSE data. Panel (a) shows detected pulse frequencies at 1-day intervals using techniques described in Bildsten et al. (1997). Panels (b) and (c) show the 99.9% confidence pulse frequency detections at 4-day intervals using our “advanced” search technique that accounts for aperiodic noise from Cygnus X-1. The orbit of Stollberg et al. (1999) was used for panels (a) and (b), while panel (c) used our new orbital parameters in Table 2, row 5, which considerably reduce the scatter in the frequency measurements. An *RXTE* PCA frequency measurement is indicated by a diamond symbol. Vertical lines near the top of panel (c) denote times of H $\alpha$  measurements. Panel (d): Pulsed flux in the 20-50 keV band measured at 4-day intervals with BATSE. Upper limits (99% confidence) are shown for all 4-day intervals where pulsations were not detected.

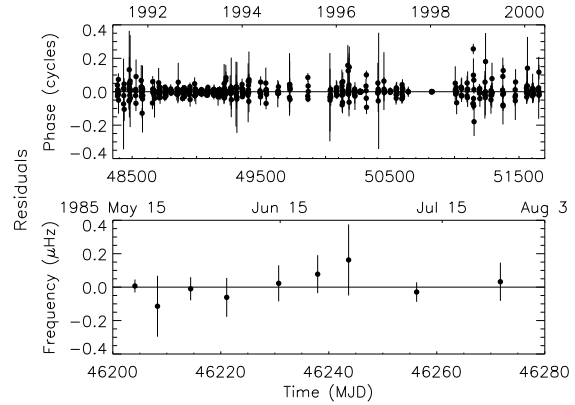


Fig. 2.— Pulse phase residuals from BATSE and *RXTE* data (top panel) and frequency residuals from *EXOSAT* data (bottom panel) resulting from our joint fit to these data. The resulting orbital parameters are listed in Table 2, row 5.

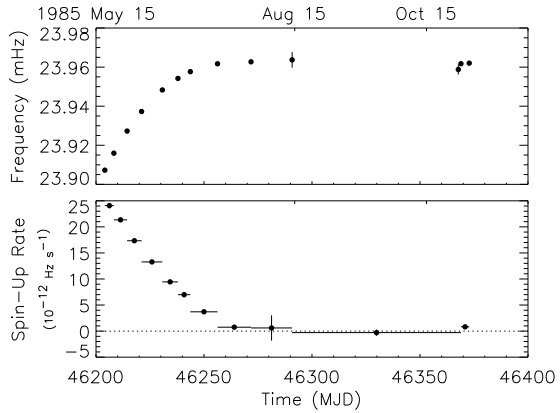


Fig. 3.— Spin frequencies and spin-up rates measured using *EXOSAT*. The top panel shows the barycentered pulse frequency corrected for the orbit in row 5 of Table 2 for the 13 observations where pulsations were detected. The bottom panel shows the spin-up rate computed by differencing adjacent frequency measurements and dividing by the corresponding time difference (denoted with horizontal lines). The spin-up rate measurement from 1985 October 29-30 (MJD 46367-68) is not plotted because it had an error of  $2.4 \times 10^{-11}$  Hz  $s^{-1}$ , due to the short duration of the October 29 (MJD 46367) observation ( $< 3000$  seconds) and due to the short, 1.2 day, spacing between the two observations.

TABLE 1—*Continued*

Number <sup>a</sup>	Start Date (MJD)	End Date (MJD)	Start Date (Calendar)	Stop Date (Calendar)
72	51651	51657	2000 Apr 17	2000 Apr 23
73 <sup>g</sup>	51691	51707	2000 May 27	2000 Jun 12
74 <sup>g</sup>	51740	51751	2000 Jul 15	2000 Jul 26
75 <sup>g</sup>	51775	51795	2000 Aug 19	2000 Sep 8
76 <sup>g</sup>	51835	51847	2000 Oct 18	2000 Oct 30
78 <sup>g</sup>	51927	51935	2001 Jan 18	2001 Jan 26
79 <sup>g</sup>	51972	51976	2001 Mar 4	2001 Mar 8
80 <sup>g</sup>	52015	52028	2001 Apr 16	2001 Apr 29
81 <sup>g</sup>	52063	52072	2001 Jun 3	2001 Jun 12
82 <sup>g</sup>	52111	52123	2001 Jul 21	2001 Aug 2

<sup>a</sup>Periastron passage number since *CGRO* launch.

<sup>b</sup>Outburst dates from *EXOSAT* detections.

<sup>c</sup>Outburst dates from *Ginga* detections.

<sup>d</sup>Included in orbit fit of Stollberg et al. (1999)

<sup>e</sup>Outburst dates from *RXTE* PCA detections.

<sup>f</sup>*RXTE* PCA detected outburst used in all orbit fits.

<sup>g</sup> $\gtrsim 3\sigma$  detections with the *RXTE* ASM. Not used in orbit fitting.

TABLE 2  
EXO 2030+375 ORBIT FITS

Fit <sup>a</sup>	$P_{\text{orb}}$ (days)	$T_{\text{peri}}$ (JD)	$a_x \sin i$ (lt-sec)	e	$\omega$	$\chi^2/\text{dof}$
S99 <sup>b</sup>	$46.02 \pm 0.02$	$2448937.0 \pm 0.2$	$262 \pm 24$	$0.37 \pm 0.02$	$223^\circ.5 \pm 4^\circ.3$	103.31/102
R only	46.02(fixed)	$2450271.5 \pm 0.2$	$236.7 \pm 6.2$	$0.416 \pm 0.004$	$206^\circ.9 \pm 6^\circ.3$	15.25/16
R+13 B	$46.026 \pm 0.003$	$2450179.56 \pm 0.02$	$241.5 \pm 3.9$	$0.414 \pm 0.004$	$212^\circ.0 \pm 0^\circ.6$	174.9/147
2 R+51 B	$46.023 \pm 0.001$	$2450317.61 \pm 0.02$	$241.4 \pm 3.5$	$0.413 \pm 0.003$	$211^\circ.1 \pm 0^\circ.6$	549.0/333
E +2 R +51B	$46.0214 \pm 0.0005$	$2450547.72 \pm 0.02$	$235.8 \pm 1.8$	$0.419 \pm 0.002$	$211^\circ.2 \pm 0^\circ.6$	556.3/338

<sup>a</sup>Fit column designates number of outbursts used from each of 3 instruments, B=BATSE, E=*EXOSAT*, and R=*RXTE* for fits in this paper.

<sup>b</sup>Orbital parameters from Stollberg et al. (1999).

TABLE 3  
DETAILS OF SPECTROSCOPIC OBSERVATIONS

Date	MJD	Telescope	Spectral Resolution (Å/pixel)	$H\alpha$ Equivalent Width (Å)
7 Sep 1986	46680	INT	2.03	-15.0
2 Oct 1992	48897	WHT	2.72	-20.2
29 Jun 1993	49167	WHT	1.33	-18.0
9 Jul 1996	50273	WHT	0.50	-6.8
1 Aug 1997	50661	WHT	0.40	-5.8
15 Jul 1998	51009	WHT	0.40	-8.0

NOTE.—The telescopes referred to are : INT - Isaac Newton Telescope, WHT - William Herschel Telescope. Both telescopes are located on the island of La Palma, Spain.

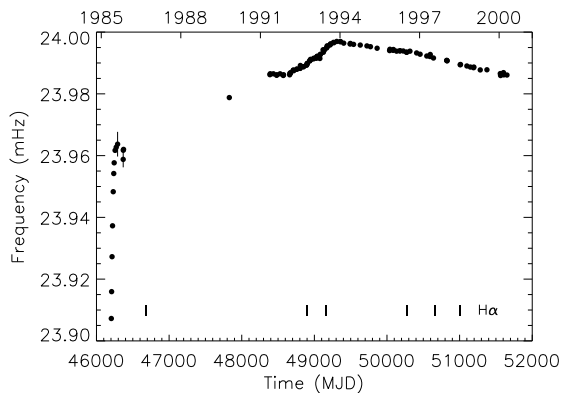


Fig. 4.— Long-term spin frequency history for EXO 2030+375. All frequencies are barycentered and corrected for the pulsar’s orbital motion using the parameters in row 5 of Table 2. Vertical lines near the bottom of the plot denote times of H $\alpha$  measurements.

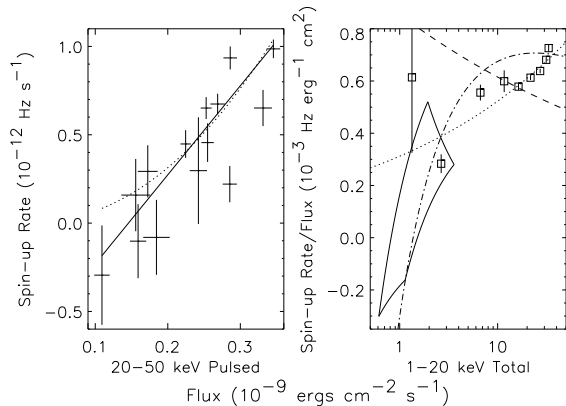


Fig. 5.— (left-hand panel): The average spin-up rates versus the average 20-50 keV pulsed fluxes on a linear scale for the brighter outbursts observed with BATSE. The solid and dotted lines are the best-fit linear and power law models, respectively, to the BATSE data. (right-hand panel): *EXOSAT* spin-up rates divided by the 1-20 keV total flux vs. the 1-20 keV total flux. The point with the largest error bar is from the normal outburst observed with *EXOSAT*, while the rest are from the giant outburst. Our best-fit power law, with an index of 1.17, and a power law with a fixed index of 6/7 are denoted by dotted and dashed lines, respectively. The dot-dashed line is the (Ghosh & Lamb 1979) model fitted to the *EXOSAT* data by (Reynolds et al. 1996). The solid box denotes the projection of the linear fit to the BATSE data assuming a range of bolometric corrections from 5.6-10.4, based on our estimated correction of 8.0 with an assumed systematic error of 30%.

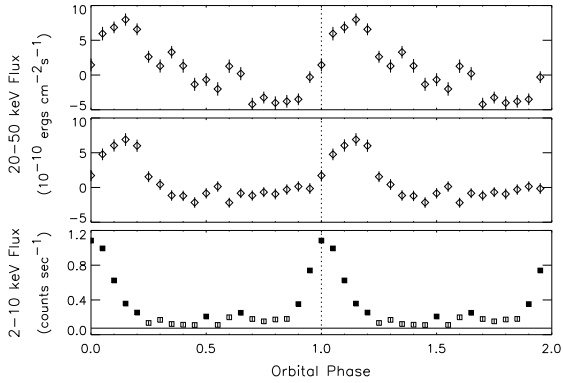


Fig. 6.— (Top 2 Panels): Epoch-folded profiles of BATSE Earth occultation data from MJD 48363-49353 (1991 April - 1993 December). A period of 46.0214 days was used with a periastron epoch of MJD 50547.22. The top panel includes rising occultations only and the center panel includes only setting occultations. The negative offset in flux is due to interference from primarily Cyg X-1 and Cyg X-3. (Bottom Panel): Epoch-folded profiles of *RXTE* ASM measurements of 2-10 keV flux from MJD 50135-52138 (1996 February - 2001 August). A period of 46.0214 days was used with a periastron epoch of MJD 50547.22. The horizontal line denotes the 1 mCrab ( $0.075 \text{ counts s}^{-1}$ ) positive bias seen in long-term averages of ASM data. The orbital phase of periastron is denoted with a dotted vertical line in all 3 panels.

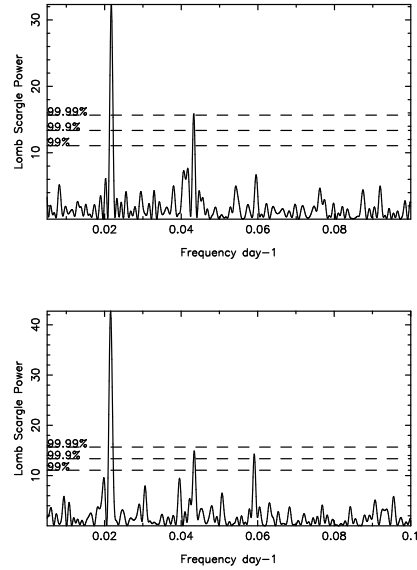


Fig. 7.— Lomb-Scargle periodograms of BATSE Earth occultation data from MJD 48363-49353 (1991 April - 1993 December). The top panel includes rising occultations only and the bottom panel includes only setting occultations. The confidence levels shown have been determined by running multiple sets of randomized data with the same window function as the BATSE data and the same statistical properties. The highest peak in each panel is near the 100% confidence level. The second highest peak is at 99.99% and 99.95% confidence in the top and bottom panels respectively.

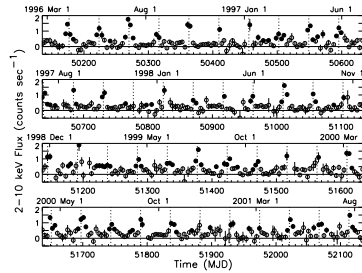


Fig. 8.— 2-10 keV flux measured with the *RXTE* ASM. The ASM measurements have been averaged over 4-day intervals. Filled circles denote  $\geq 3\sigma$  detections. Vertical dotted lines denote periastron passage times.

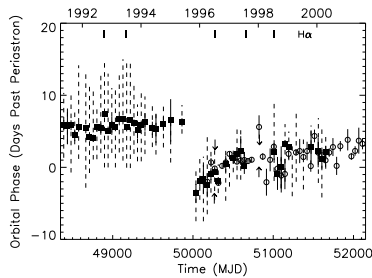


Fig. 9.— Orbital phase of EXO 2030+375 outburst peaks versus time from 1991 April - 2001 August. Dashed lines indicate the orbital phases when pulsations from EXO 2030+375 were detected with BATSE. Filled squares indicate the times of outburst peaks estimated from Gaussian fits to 1-day BATSE pulsed fluxes corresponding to BATSE pulsed phase measurements. Open circles indicate the times of outburst peaks estimated from Gaussian fits to 46.0214 days of single dwell *RXTE* ASM 2-10 keV flux measurements centered on the periastron epoch for each outburst. Arrows denote the orbital phase range of *RXTE* PCA detections. Vertical lines near the top of the plot denote times of  $H\alpha$  measurements.

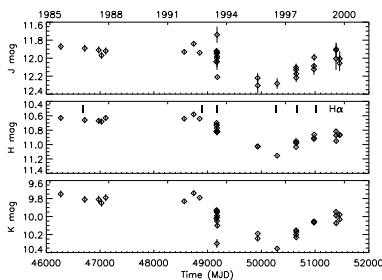


Fig. 10.— Long-term IR history of the optical counterpart to EXO 2030+375. The JHK magnitudes remain approximately constant from the giant outburst observed with *EXOSAT* in 1985 until the BATSE observations (1991-2000). After about MJD 49000 (1993 January), the JHK magnitudes begin to decline, dropping to a minimum near MJD 50300 (1996 August), followed by a slow brightening. Vertical lines near the top of the center panel denote times of  $H\alpha$  measurements.

### EXO 2030+375 H alpha spectra

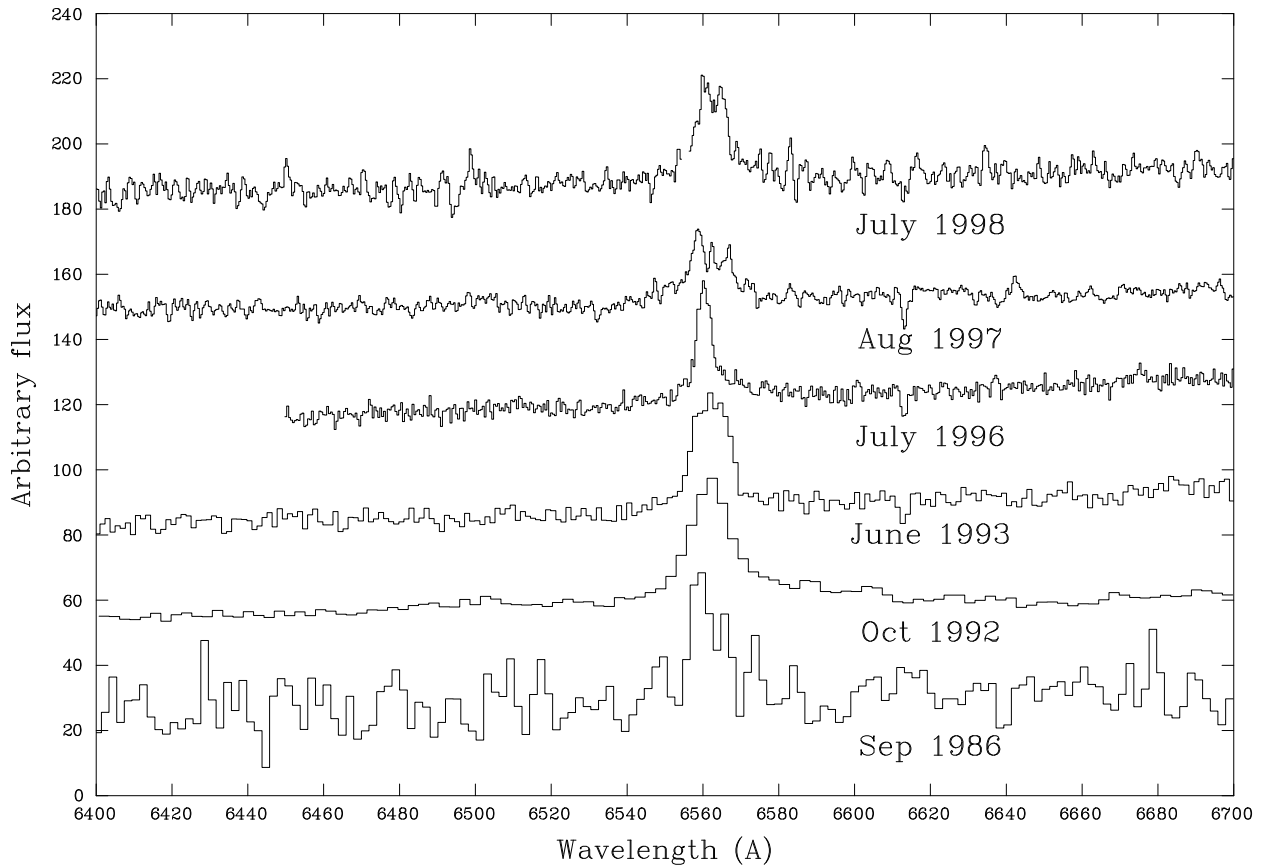


Fig. 11.—  $H\alpha$  line profiles from 6 observations of EXO 2030+375. Times of the  $H\alpha$  profiles are denoted with vertical bars in Figures 1, 4, 9, and 10. The extended nature of the 1997 (MJD 50661) and 1998 (MJD 51009) profiles suggests a different circumstellar disk structure than before. The 1996 (MJD 50273), 1997, and 1998 data were taken with almost the same instrumental configuration and hence are directly comparable. The earlier data were taken with poorer wavelength resolution. (See Table 3.)